DOI:
10.1016/bs.ctm.2015.12.002

Document Version
Peer reviewed version

Voltage-gated sodium channels: mechanistic insights from atomistic molecular dynamics simulations

Victoria Oakes,[1] Simone Furini,[2] Carmen Domene[1,3]

[1]Department of Chemistry, Britannia House, 7 Trinity Street, King's College London, London SE1 1DB, U.K.

[2] Department of Medical Biotechnologies, University of Siena, viale Mario Bracci 16, I-53100, Siena, Italy

[3]Chemistry Research Laboratory, Mansfield Road, University of Oxford, Oxford OX1 3TA, U.K.

Contents

Abstract

The permeation of ions and other molecules across biological membranes is an inherent requirement of all cellular organisms. Ion channels, in particular, are responsible for the conduction of charged species, hence modulating the propagation of electrical signals. Despite the universal physiological implications of this property, the molecular functioning of ion channels remains ambiguous. The combination of atomistic structural data with computational methodologies, such as molecular dynamics (MD) simulations, is now considered routine to investigate structure-function relationships in biological systems. A fuller understanding of conduction, selectivity and gating, therefore, is steadily emerging due to the applicability of these techniques to ion channels. However, because their structure is known at atomic resolution, studies have consistently been biased toward K^+-channels, thus the molecular determinants of ionic selectivity, activation and drug blockage in Na^+-channels are often overlooked. The recent increase of available crystallographic data has eminently encouraged the investigation of voltage-gated sodium (Na_V) channels via computational methods. Here, we present an overview of simulation studies that have contributed to our understanding of key principles that underlie ionic conduction and selectivity in Na^+-channels, in comparison to the K^+-channel analogs.

Keywords: ion channels, permeation, selectivity, conduction, free energy methods

Abbreviations

PD: pore domain

SF: selectivity filter

TRP: transient receptor potential

VGIC: voltage gated ion channel

VSD: voltage sensor domain

1 Introduction

Ion channels are an important family of integral membrane proteins that are responsible for passive transport across biological membranes. Gene sequencing has identified over 400 alleged ion channels, yet only a fragment of these have been cloned, functionally tested, and crystalized (Bagal et al., 2013). Therefore, despite their ubiquitous distribution in tissues throughout all living organism and their decisive roles in fundamental processes such as cell proliferation, nerve transmission and muscle contraction, sensory transduction and blood pressure regulation ion channels are considerably underexploited by targeted drug therapies, (Bagal et al., 2013). Furthermore, conglomerates of ailments, known as 'channelopathies', are the consequence of ion channel mutations and subsequent functional alterations (Zaydman, Silva, & Cui, 2012).

The widespread physiological implications of ion channels emanate from the modulation of electrical signals across the cellular membrane. This occurs by facilitating the passive diffusion of ionic species down their electrochemical gradient between periplasmic and cytoplasmic compartments. The permeation pathway is ordinarily 'gated' on the application of external stimuli; for example, adjustment of transmembrane potentials (voltage-gated ion channels), ligand binding (ligand-gated ion channels) and mechanical stretch (mechanosensitive channels) can induce transformations between open and closed states. A constricted region of the pore, known as the selectivity filter, imposes further restraints on conduction, by discrimination between ionic species. Selectivity, as this property is known, is responsible for K^+/Na^+ permeability ratios of 1000:1 and 1:8 in K^+ and Na^+-channels respectively (Hille, 1992).

The understanding of such channel properties at the atomic level using computational techniques has traditionally been focused toward K^+ channels due to the availability of crystallographic data, while the principles determining conduction in Na^+ channels remain largely unsolved. The publication of the crystal structure of the Na_VAb α-subunit, (Payandeh, Scheuer, Zheng, & Catterall, 2011) a mutated voltage-gated Na^+ channel from *Arcobacter butzleri* (Figure 1.a), and subsequent

analogous structures from bacterial sources (Bagnéris et al., 2013; McCusker et al., 2012; J. Payandeh, Gamal El-Din, Scheuer, Zheng, & Catterall, 2012; Shaya et al., 2014), in the last five years has invigorated interest into the workings of Na^+ channels, resulting in numerous exploratory computational studies. In this Chapter, we provide a comprehensive survey of the available X-ray crystal data and accompanying simulation studies that have been undertaken to discern the fundamental features regulating permeation and selectivity in Na^+ channels, with particular focus on voltage-gated sodium (Na_V) channels. The atomic structures of associated β-subunits have recently been determined (Gilchrist, Das, Van Petegem, & Bosmans, 2013; Namadurai et al., 2014), yet in this review, the focus is on the principal subunits (designated α or α1) which are responsible for the voltage-gated ion conductance which is the defining characteristic of these proteins.

2 Voltage-Gated Sodium Channels

Na_V channels form part of the voltage-gated ion channel (VGIC) family, which contains a variety of potassium, sodium, calcium, chloride and transient receptor potential (TRP) ion channels, of which Na_V was the first to be cloned (Noda et al., 1984). Currently, based on common structural and functional properties, with distinct expression, regulatory and pharmacological profiles nine members of the Na_V family have been identified ($Na_V1.1$-$Na_V1.9$).

Na_V channels are critical for the generation of action potentials in neurons and other excitable cells. Most biological membranes experience a high-Na^+/low-K^+ concentration on the extracellular surface, and a low-Na^+/high-K^+ concentration on the intracellular surface, generating apt conditions for passive Na^+ influx and K^+ efflux in their respective channels. At typical negative resting potential (i.e. -60 mV), both K_V and Na_V activation gates are closed. Under depolarizing conditions, Na_V channels open allowing diffusion of Na^+ ions through the central pore; this causes further depolarization inducing a large inward current. K_V channels respond slower than Na_V channels to depolarization, therefore, delayed K^+ efflux is observed and an overall positive membrane potential results. At the peak of depolarization, repolarization is initiated by the inactivation of Na_V and the opening of K_V channels.

By the generation of a nascent electrical signal in this way, VGICs initiate action potentials in excitable cells in various tissues in the heart, brain and nervous system.

The expression on Na_V channels is not limited to excitable cells; the role of Na_V channels in astrocytes, NG2 cells, microglia, macrophages and cancer cells is currently under investigation (Black & Waxman, 2013). The dysfunction of Na_V channels has been affiliated with a myriad of disorders such as pain, migraine, impaired movement, epilepsy and cardiac arrhythmias (Mantegazza, Curia, Biagini, Ragsdale, & Avoli, 2010). Currently, treatment of these disorders is serviced by the binding of small organic molecules, such as local anesthetics, to block the channels (Bagal et al., 2013). However, due to the high structural and sequence homology (Figure 2), subtype targeting can rarely be achieved, increasing the risk of inimical side effects (England & de Groot, 2009). Therefore, understanding of the molecular determinants of conduction, gating and drug binding in ion channels is required to develop the next generation of subtype specific pharmaceuticals.

3 Structural Basis of K^+ vs Na^+ Conduction

Hodgkin and Keynes provided the first insights into conduction in K^+ channels, proposing a 'knock-on' mechanism of ionic conduction, associated with concerted transitions of individual ions in a single-file manner through a narrow pore (Hodgkin & Keynes, 1955). In addition, various theories for selectivity were proposed concerning the hydration free energy (Eisenman, 1962; Eisenman & Horn, 1983), coordination number and the size difference of K^+ and Na^+ ions (Bezanilla & Armstrong, 1972). Furthermore, sequence analysis, and complementary mutagenesis studies of K^+ channels identified a conserved sequence, TVGYG, which confers ionic selectivity, hence coined the selectivity filter (Heginbotham, Lu, Abramson, & MacKinnon, 1994; Smart, Goodfellow, & Wallace, 1993). The X-ray crystal structure of KcsA, from *Streptomyces lividans*, provided the first atomistic structural information, revealing key insights into the conduction/selectivity mechanisms of K^+ channels (Doyle et al., 1998). Developments concerning expression, purification and crystallization of ion channels have now lead to a wealth of available K^+ channel crystal structures (Brohawn, del Marmol, & MacKinnon, 2012;

Doyle et al., 1998; Jiang et al., 2003; Kuo et al., 2003; Long, Campbell, & Mackinnon, 2005; Miller & Long, 2012). K^+ channels can exist in numerous activation states, most simply defined as open, closed and inactivated. A range of these is sampled throughout these structures, providing additional clues into the gating mechanism of K^+-channels.

Throughout K^+ channels, a fundamental pore structure is conserved. The channel is formed from a symmetrical arrangement of four identical subunits composed of inner and outer transmembrane α-helices connected by a pore loop. The latter contains a pore helix and the signature selectivity sequence, TVGYG. A water-filled cavity, directly connected to the cytoplasm, is present underneath the selectivity filter to overcome large energetic barriers accompanying penetration of the hydrophobic core of the surrounding membrane by ionic species (Parsegian, 1969). In the open state of the channel, passage of ions is unrestricted from the cavity to the cytoplasm. In the closed state, the inner helices coalesce, via bending at a conserved glycine residue, preventing ion translocation and intra- and extracellular water exchange. A wide range of external stimuli modulates cytoplasmic gating of this sort, interceded by supplementary structural domains in some cases.

In K_V channels, an additional four transmembrane segments in each subunit comprise the voltage sensor domain (VSD), which regulates channel opening. The molecular basis of voltage sensing and gating was elucidated by the X-ray crystal structure of K_VAP from *Aeropyrum pernix* at 3.2 Å resolution with the isolated voltage sensor domain (VSD) at 1.9 Å (Jiang et al., 2003). The VSD segments, denoted S1-S4, arrange in an anti-parallel α-helical bundle, attached to the 'traditional' pore helices, S5-S6. Between four and seven repeat motifs containing a positively charged residue, ordinarily arginine, succeeded by two hydrophobic residues constitutes the conserved S4 VSD segment that is deemed the activation gate (Stuhmer et al., 1989) The assemblages of charge clusters in this region stabilize S4 within the membrane and facilitate channel gating by interactions with S1 to S3 (Long, Tao, Campbell, & MacKinnon, 2007). When stimulated by a change in the transmembrane voltage, movement of S4 prompts rearrangement of the pore-lining helices, via the S4-S5

linker, thus controlling the passage of ions.

Ion permeation, of ionic species other than K^+, is blocked at the selectivity filter. The KcsA structure, revealed a selectivity filter optimized for favorable binding and efficient conduction of K^+ ions. In physiological K^+ concentrations, the selectivity filter residues arrange to form rings of carbonyl oxygen atoms directed toward the center of the pore axis (Figure 1.b). With the added contribution of threonine side-chain oxygen atoms, four adjoining sites are formed, namely S1-S4, which are able to bind dehydrated ions in a cage-like structure. Further binding sites for 'partially' hydrated K^+ have been identified at the extracellular entrance (S_0, S_{EXT}) and within the central cavity (S_C). Stabilization of ions in S_C is a consequence of the helix-dipole effect from the above pore-helices (Aqvist, Luecke, Quiocho, & Warshel, 1991; S. Furini, Zerbetto, & Cavalcanti, 2007; Jogini & Roux, 2005). Specific salt bridges and hydrogen bonding with proximal helices and solvent generally stabilize the selectivity filter (Cordero-Morales, Jogini, Chakrapani, & Perozo, 2011). However, a further KcsA structure, in low K^+/high Na^+ concentrations, displayed significant distortions in the selectivity filter rendering the channel impermeable to K^+, Na^+ and even water (Zhou, Morais-Cabral, Kaufman, & MacKinnon, 2001). This structure has been associated with an inactivated state, reminiscent of C-type inactivation, a mechanism of gating characterized by conformational changes in the proximity of the selectivity filter which prevent conduction (Cuello, Jogini, Cortes, & Perozo, 2010).

In contrast to K_V channels, the molecular structure of eukaryotic Na_V channels remains uncharacterized. Crystallographic data of bacterial Na_V channels, of which the first structure, [mutant] Na_VAb, was published in 2011 (Payandeh et al., 2011) with numerous full length (Na_VRh, wild-type Na_VAb) (Bagnéris et al., 2013; J. Payandeh et al., 2012; Xu Zhang et al., 2012) and pore only structures to follow (Na_VMs, Na_VAe1p) (McCusker et al., 2012; Shaya et al., 2014) have provided, to date, the greatest molecular insights of Na_V channels at the atomic level.

Bacterial Na_V channels, display a conserved structure similar to that of K^+ channels (Figure 1.a). As noted previously, four identical subunits arranged around a large

central cavity, that can accommodate and stabilize hydrated ions. The P-loop region contains a similar α-helix, with the addition of a unique second pore-helix in an anti-parallel configuration (**Figure 1**.a). The available structures display remarkable similarities with Cα superposition of monomer subunits comfortably under 1 Å in most cases (Payandeh & Minor Jr, 2015), and only subtle differences in the symmetry of the pore helices with respect to the pore axis (Simone Furini & Domene, 2013).

A novel finding in Na_VAb pore architecture is the presence of lateral openings, termed fenestrations, directly connecting the central pore to the surrounding membrane. In Na_VAb, membrane phospholipids penetrate these cavities, providing a further physical block to conduction in the pore (Payandeh et al., 2011). Furthermore, these fenestrations may provide an additional entry route for small neutral or hydrophobic molecules and will therefore have implications for targeted channel blockage. Analogous fenestrations have recently been identified in multiple members of the two-pore domain K^+-channel (K_{2P}) family (Brohawn et al., 2012; Miller & Long, 2012).

The Na_V VSDs are analogous to those found in K_v channels. In Na_VAb, interactions of S4 with conserved intracellular and extracellular charge clusters suggest that the VSD is in an activated conformation (Payandeh et al., 2011). Therefore, Na_VAb is in a supposed 'pre-open' state in which the VSD is in an active state yet the cytoplasmic entrance is closed. Subtle differences in the conformational, and hence activation, state are observed throughout the available Na_V VSD structures; perspectives on voltage-sensing mechanisms as a consequence of these observations are outlined in a recent review by Payandeh et al (Payandeh & Minor Jr, 2015).

The resolved selectivity filter structure has also provided significant contributions to the understanding of Na^+ conduction. The sequence and structure is clearly divergent from K^+ channels, being notably wider and shorter, and comprised of four amino acids whose side chains partially line the pore (Figure 1.c). An arrangement of four glutamates, the so-called EEEE ring, forms the mouth of the selectivity filter in Na_VAb, consistent with experimental studies that implicated an anionic region of

high-field strength (Hille, 1971, 1972) composed of Glu side-chains (Heinemann, Terlau, Stuhmer, Imoto, & Numa, 1992a; Sun, Favre, Schild, & Moczydlowski, 1997a), in the selective conduction of Na^+ over K^+. The equivalent sequence in eukaryotic sodium channels, the DEKA motif, has also been affiliated with channel selectivity by mutagenesis studies (Favre, Moczydlowski, & Schild, 1996; Sun, Favre, Schild, & Moczydlowski, 1997b). Sequence alignments of the selectivity filter and surrounding pore domain in select bacterial (Na_VAb, Na_VRh, Na_VMs, NaVAe1p) and mammalian ($Na_V1.1$, $Na_V1.4$) channels are shown in Figure 2.

Na_VAb (with mutations I217C and M221C) and Na_VMs displayed symmetrical selectivity filter structures as above, and are therefore considered conductive states. However, Na_VRh (X. Zhang et al., 2012) contains a dissimilar selectivity filter sequence, TLSSWE substituting TLESWS; therefore, the outer ring is comprised of serine residues, which adopt non-uniform conformations resulting in a 1-2 Å reduction in selectivity filter radii. Notable asymmetry is also observed in wild-type Na_VAb. Therefore, both are thought to correspond to inactivated states.

Despite the inability to resolve the location of Na^+ ions within the selectivity filter, on the basis of structural data three binding sites were proposed in Na_VAb. Firstly, the side chain of Glu177 (S_{HFS}) provides a negatively charged region at the extracellular entrance that can feasibly attract positively charged ions. Deeper sites formed of rings of carbonyl atoms from Leu76 (S_{CEN}) and Thr175 (S_{IN}) are proposed to form the remainder of the permeation pathway, with the latter sites potentially binding Na^+ ions via hydrogen bonding with a square array of water molecules forming the ions solvation shell. All binding sites are, therefore, amenable to hydrated ions, suggesting that in stark contrast to K^+ channels, sodium ions can traverse the entire length of the channel without full desolvation.

It is worth noting that all published structures to date are of prokaryotic origin; eukaryotic Na_V channels are comprised of a single polypeptide chain containing over ~2000 amino acids, arranged into four homologous transmembrane domains. A schematic representation of the basic topology of voltage-gated sodium channels from prokaryotic and eukaryotic origins is presented in Figure 2. The general

representation of Na_V channel architecture from bacterial channels shows four homologous subunits comprising voltage-sensor (S1-S4) and pore-forming (S5-S6) domains, containing the signature EEEE sequence (**Figure 2**). Further differences may be observed in eukaryotic species where the equivalent selectivity filter ring sequence is DEKA in contrast with EEEE (Na_VAb) and SSSS (Na_VRh). Note that eukaryotic channels share a similar tetrameric architecture, yet in a continuous a polypeptide chain, with non-conserved sequences in individual domains. Therefore, crystallization of eukaryotic channels will markedly aid the advancement of this field.

4 Overview of Computational Studies

Crystallographic data essentially only provides static structural information, with limited indications of the operations in a biological setting. Therefore, computational studies utilizing Molecular Dynamics (MD) simulations are employed to supplement experimental data and gain time-dependent information on biological systems.

In MD simulations, integration of Newton's equations of motion, via an initial potential energy function, yields a trajectory containing the time evolution of the system. Accordingly, dynamical information can be gained at the atomistic level. The analytic expression for the energy, known as the *forcefield*, is composed of numerous functions approximating inter- and intramolecular energetic contributions. Various forms of this expression have been developed for simulations of biological molecules, including, but not limited to, the CHARMM (Chemistry at Harvard Molecular Mechanics) (Brooks et al., 1983), AMBER (Assisted Model Building with Energy Requirement) (Cornell et al., 1995), GROMACS (Groningen Machine for Chemical Simulation) (Berendsen, van der Spoel, & van Drunen, 1995) and OPLS (Optimized Potentials for Liquid Simulations) (Jorgensen & Tirado-Rives, 1988) forcefields. The availability of forcefield parameters for proteins, lipids, ions and water, alongside defined protocols for the parameterization of novel drug molecules, equips the user with appropriate tools to study the behavior of ion channels embedded in model membranes and the identification of potential drug binding sites, for example.

The availability of accurate forcefields is the first necessary condition for the analysis

of ion conduction by atomistic simulations, the second one being the possibility to obtain statistically robust estimates of the conduction properties by sampling the ion configurations with MD trajectories. The most direct method to sample ion configurations in an MD trajectory is certainly to simulate the ion channel in the presence of an electrochemical driving force, and to observe ion conduction as it happens. In simulations with periodic boundary conditions, a straightforward strategy for simulating the presence of a driving force is to apply a constant electric field in the direction orthogonal to the membrane (Gumbart et al., 2011). An alternative strategy is to include in the simulation domain two parallel lipid membranes, which divide the space in two separate compartments. In this way, it is possible to impose an electrochemical gradient between the two sides of each membrane by controlling the ion concentrations in the two compartments (Kutzner, 2011). In order to analyze ion conduction by these strategies it is necessary to simulate trajectories sufficiently long to sample numerous conduction events. For a typical ion channel (conductance 10-50 pS) at physiological condition (membrane potential in the range ±100 mV) it is necessary to simulate tens of microseconds in order to obtain a statistical robust estimate of the conductance. A different approach for the analysis of the conduction properties of an ion channel is to estimate the potential of mean force (PMF) along a restricted set of reaction coordinates. Several algorithms exist to accelerate sampling along a pre-defined set of reaction coordinates. 'Umbrella sampling' which uses a biased potential to transform a system between thermodynamic states has been widely used in the field of ion channels, but examples of applications of other approaches, such as metadynamics (Stock, Delemotte, Carnevale, Treptow, & Klein, 2013), adaptive biasing force (Henin et al. 2008), or steered-MD (Ngo et al. 2014) were also reported in the literature. Compared to the direct sampling of ion conduction in simulations with a driving force, the computational cost of PMF calculations might be significantly lower. However, these methods do not provide a direct estimate of the channel conductance, and the choice of the reaction coordinates might be critical.

MD simulations, and accompanying techniques, have become established methods to study K^+-channels in atomistic detail. We direct the reader to accomplished

reviews (Simone Furini & Domene, 2013; Roux, 2005) for an extensive overview of this field, yet we highlight a notable success in determining the conduction mechanism: the predominant selectivity filter conformations hinted by the structural studies (Morais-Cabral, Zhou, & MacKinnon, 2001), w-S2-w-S4 and S1-w-S3-w, were identified in multiple MD simulations (Bernèche & Roux, 2000; Domene, Klein, Branduardi, Gervasio, & Parrinello, 2008; C. Domene & Sansom, 2003) and confirmed by free energy perturbation (FEP) techniques (Aqvist & Luzhkov, 2000) leading to the recognition of a 'knock-on' mechanism, driven by the approach of K^+ from the central cavity and subsequent ion-ion repulsion, summarized in Figure 3 (Morais-Cabral et al., 2001). Free energy calculations later showed that cation pairs moving through the selectivity filter without intervening water molecules are energetically feasible (Furini & Domene, 2009). In this mechanism, in addition to direct K^+-K^+ contacts, vacancies are also involved during the permeation event. A schematic representation of both mechanisms is illustrated in Figure 3. FEP methods were also used to demonstrate a significant energetic preference for K^+ over Na^+ in the selectivity filter of K^+-channels (Berneche & Roux, 2001; Noskov & Roux, 2006). Specifically, S2 was identified as a highly selective, S1 and S3 displayed moderate selectivity whereas S4 provided a non-selective site, giving insights into the molecular determinants of selectivity in K^+ channels (Luzhkov & Åqvist, 2001).

Technical progressions concerning the development of parallel computing algorithms have resulted in an expansion of the phenomena that can be sampled throughout molecular simulations. D.E. Shaw and colleagues have been instrumental in enabling the performance of long-scale simulations of ion channels by the construction of the supercomputer Anton, which performs over an order of magnitude faster than any other machine utilizing an MD code. Simulations on an extended timescale under the influence of different membrane potentials have allowed the first direct observation of an ion channel gating transition (Jensen et al., 2012).

It is also worth noting that the Lennard-Jones interaction parameters in non-polarizable *forcefields* are derived from the standard Lorentz-Berthelot combination

rule optimized to emulate the free energies of ions in bulk water, therefore, in heterogeneous environments, such as the cell membrane, this method has inherent limitations. Therefore, the continued improvement of polarizable forcefields will enhance the accuracy to which ion permeation can be simulated (Illingworth & Domene, 2009; Vanommeslaeghe & MacKerell Jr, 2015; Xu et al., 2015).

4.1 Application to Na_V Channels

Following the publication of the Na_VAb structure, numerous studies began to emerge in an attempt to identify the molecular determinants of Na^+ conduction mechanism, employing the vast range of available methods. In what follows, an exhaustive review of the MD studies that have been published to date is provided, placing particular emphasis on the atomistic structure of the central pore that has key implications for conduction and selectivity.

The first published MD simulations demonstrated the original Na_VAb structure was stable in the presence and absence of Na^+ ions (Carnevale, Treptow, & Klein, 2011). The cytoplasmic gate remained closed for the duration of the simulations; therefore access to the central pore was limited to entrance at the periplasmic side, via the selectivity filter. Observed ion dynamics confirmed earlier binding site predictions (Figure 4). In Na^+-channels binding sites for hydrated or partially hydrated sodium ions have been identified at the extracellular entrance (S_{HFS}), in the core region of the selectivity filer (S_{IN} and S_{CEN}) and within the central cavity (S_C). A considerable occupation time was observed at S_{HFS} (~10 ns), comprised of both symmetric and asymmetric conformations, with the former predominant. Electrostatic interactions with two opposite Glu177 residues, H-bonding between coordinating water molecules and remaining Glu177 residues, and further interactions with surrounding water stabilized ions in the on-axis binding mode. In contrast, the ion preferentially contacts one Glu177 and adjoined Ser178 in the off-axis mode at this site. The overall octahedral geometry mimics that observed in sodium hydrate crystals. Ions were observed to traverse deeper into the selectivity filter, mediated by surrounding water molecules to bind at S_{IN} via S_{CEN}, as postulated from the crystal structure. It is apparent that favorable binding sites are established on the basis of retaining a full

hydration shell, with contributions from both water molecules and protein atoms in a manner consistent with K^+ conduction through Kv channels. In contrast, ions are partially hydrated throughout and interact in an asymmetric fashion to lining residues. Finally, water permeation is apparently uncoupled to the presence of bound species and therefore ion permeation. The nature of water transport in K^+ channels remains controversial in the literature robust water flux has been observed in a K^+ depleted channel (Furini, Beckstein, & Domene, 2009), contrary to various accounts suggesting ions and water molecules are transported on a 1:1 ratio.

The Na_VAb binding sites of channels were also corroborated by the presence of defined energy minima in single and multi-ion potential of mean force conduction profiles (Corry & Thomas, 2012; Furini & Domene, 2012) and various normal and long scale MD simulations. A successive study provided insights into the stability of these binding sites; the overall selectivity filter structure remained remarkably similar in numerous ionic configurations, albeit a constriction of the pore in the presence of ions that can be attributed to favorable electrostatic interactions (Qiu, Shen, & Guo, 2012). This renders evidence the selectivity filter is stable independent of ionic occupancy, contrasting with K^+ channels that exhibit significant distortions in the absence of K^+ ions (Domene et al., 2008; Furini & Domene, 2009; Zhou et al., 2001).

Simulations of Na_V orthologs confirmed conserved selectivity filter binding sites across the bacterial Na_V family. The location and habitation of analogous binding sites observed in MD simulations of Na_VMs (Ke, Timin, & Stary-Weinzinger, 2014) is consistent with electron density detected in the Na_VMs crystal structure (McCusker et al., 2012). In Na_VRh, due to the non-conserved selectivity filter sequence, the characteristic inner 'EEEE ring' and outer 'SSSS ring' at the extracellular mouth are in reversed positions. Despite the supposed collapsed conformation of these residues, reorientation at the side chain of the inner ring (S181) leads to spontaneous opening of the selectivity filter in the first stages of the simulation (Zhang et al., 2013). Thereafter, occupation of binding sites at the vestibule (S181/E183 side-chains: S1) and the inner of the selectivity filter (T178/L179 backbone carbonyls: S2) is

observed.

To provide a feasible conduction pathway, an understanding of energetic barriers accompanying ionic movement, in addition to characterization of favorable binding sites is required. The application of free energy techniques to K^+ channels proved integral in elucidating the mechanism of K^+ conduction, therefore similar studies for Na_V similarly emerged. Furthermore, long scale MD simulations allow for the production of statistically significant conduction rates that can be validated against experimental single channel conductance measurements.

4.2 Single vs. Multi-Ion Conduction

The question of pore ion occupancy has ensued debate in the literature for many years, with flux measurements (Benos, Hyde, & Latorre, 1983) and reversal potentials (Begenisich & Cahalan, 1980) suggesting independent and multi- ion movement respectively, with the latter supported by Brownian dynamics (Vora, Corry, & Chung, 2008). Therefore, single and multi-ion profiles of Na^+ conduction, utilizing the Na_VAb structure, emerged from numerous research groups (Corry & Thomas, 2012; Furini & Domene, 2012).

1D PMF profiles exploring movement of a single ion as a function of the pore axis follow the expected permeation pathway, subsequently occupying S_{HFS}, S_{CEN} and S_{IN} until release into the central cavity. Due to the attractive interactions with the 'EEEE ring' a deep energy (between –5 kcal/mol (Corry, 2013) and -8 kcal/mol (Furini & Domene, 2012) relative to the extracellular solution) well is observed at S_{HFS} corresponding to the off-axis binding mode described previously. Despite maintaining a full hydration shell throughout, penetration further into the selectivity filter is accompanied by an energetic barrier of ~4 kcal/mol (Corry, 2013; Furini & Domene, 2012).

Multi-ion profiles demonstrated distinct differences; the presence of a second ion in close proximity to a bound ion in S_{HFS}, significantly lowers the barrier for selectivity filter entrance. A further reduced energy well is also observed when both S_{CEN} and S_{HFS} are occupied. Therefore, the minimum energy pathway between initial (ions

bound in the selectivity filter and external medium, denoted extracellular) and final states (ions bound in the selectivity filter and the central cavity, denoted intracellular) follows the multi-ion configurations: extracellular/S_{HFS}, S_{HFS}/S_{HFS}, S_{HFS}/S_{CEN}, S_{HFS}/S_{IN}, S_{HFS}/intracellular (Figure 5). Considering this route, permeation can occur from the extracellular region into the central cavity with an energetic cost less than 3 kcal/mol. This value is consistent with the magnitude of energetic barriers previously determined for K^+ channels and the production of high flux rates (Aqvist & Luzhkov, 2000; Berneche & Roux, 2001).

Further efforts to characterize permeation through the Na_VAb selectivity filter were undertaken using metadynamics simulations (Stock, Delemotte, et al., 2013). Binding as a function of the radial distribution around the pore axis, as well as the distance along the pore axis, was taken into consideration to analyze previously unexplored two-ion configurations, and hence alternative conduction pathways. In particular, this allowed inspection of doubly occupied binding sites, a possible consequence of the wide selectivity filter.

Five local minima were recognized; potential wells, relative to the uppermost sampled state, of ~-12 kcal/mol corresponded to occupancy of S_{HFS}/S_{CEN} and S_{CEN}/S_{CEN} whereas shallower regions, between -7 and -9 kcal/mol coincided with S_{HFS}/S_{HFS}, S_{HSF}/S_{IN} and S_{CEN}/S_{IN} configurations. These states form a complex network leading between the initial and final states of inward conduction, of which four are sampled in the minimum energy pathway (S_{HFS}/S_{HFS}, S_{HFS}/S_{CEN}, S_{CEN}/S_{CEN}, and S_{CEN}/S_{IN}). A direct S_{HFS}/S_{HFS} to S_{HFS}/S_{HFS} transition is also viable, in this case, illustrating transitions can be independent of the preceding ions, and conduction can occur via ‘knock-on’ or ‘drive-by’ mechanisms through the selectivity filter. These findings provide additional feasible routes to two-ion conduction, summarized in Figure 5.

Overall, it is apparent that the conduction a single Na^+ ion is promoted by the presence of additional ions. Weak coupling such as this can be described as a moderate version of the ‘knock-on’ mechanism. Indications of a conserved mechanism throughout bacterial Na_V channels have been acknowledged. For example, in Na_VRh free energy perturbation (FEP) methods were used to determine

if entrance to the outer state, would destabilize ion binding at the inner site. Binding affinity was found to diminish from 3.7 kcal/mol to 2.6 kcal/mol, hence promoting onward conduction to the central cavity.

Throughout the examples described above, further characterization of the permeation pathway succeeding the central cavity is restricted due to the closed state of the Na_VAb structure. MD simulations, in the same Stock et al study (Stock, Delemotte, et al., 2013) utilized an open-state structure of Na_VAb conferred from comparative studies of the available Na_VAb structure with activated-open and resting-closed states of $K_V1.2$ (Amaral, Carnevale, Klein, & Treptow, 2012) allowing for analysis of whole channel permeation. The onset of a hyperpolarized potential (-600 mV) to promote inward permeation events, identified an average selectivity filter occupancy of ~1.8 ions throughout, providing further evidence that in the presence of a negative potential simultaneous binding of two ions is part of the normal functioning of the channel. Furthermore, ions were found to predominantly follow the minimum energy pathway identified in the previously described metadynamics calculations.

Similarly, simulations based on pore-only channel structure from Na_VMs (McCusker et al., 2012), containing an open activation gate, also identified an average selectivity filter occupancy of ~1.8 ions (Ulmschneider et al., 2013). Both single and multi-ion binding events were observed, with the latter predominant; configurations with ions occupying an outer (extracellular site or S_{HFS}) and inner site (S_{CEN}, S_{IN} or an intermediate region 3Å below S_{HFS}) monopolizes approximately 70% of the simulation. The use of microsecond simulations, in combination with a constant electric field along the channel axis as in this study, allowed accurate estimation of conductance rate (34 ± 6 pS), in comparison to single channel conductance of transfected HEK cells (~33 pS) (Ulmschneider et al., 2013). This accordance with experimental data suggests that both conduction mechanisms are physiologically relevant, albeit to different extents. Furthermore, the rate of water transport was quantified of ~3 x 10^9 s^{-1} in both directions, with a dwell time of two orders of magnitude less than Na^+ (< 1 ns). In contrast to strongly coupled transport in K^+

channels (Alcayaga, Cecchi, Alvarez, & Latorre, 1989; Ando, Kuno, Shimizu, Muramatsu, & Oiki, 2005), this confirms earlier proposals that the permeation of water was uncoupled to that of ions in Na^+ channels.

Further large-scale MD simulations, of the Na_VAb structure, totaling ~21.6 µs equilibrium conditions (under 0 mV), provided unique insights into selectivity filter occupancy and its relation to the conformational state of the selectivity filter, specifically the EEEE motif (Chakrabarti et al., 2013). These simulations displayed direct observations of 'knock-on' and 'knock-off' conduction events. Due to the closed nature of the channel, it is likely the occupation of the central cavity is higher than expected in an open state structure in the presence of an electrochemical gradient. Analysis of the selectivity filter alone, confirmed an approximate 70% population of doubly occupied configurations, however, the identity of the remaining states digressed, with a triply occupied arrangement constituting 23%, increasing the average selectivity filter occupancy to 2.09 ± 0.05**.** The observed translocation kinetics has been attributed to the of presence highly degenerate ionic binding modes concerning the conformational isomerization of the EEEE ring. Glu177 side-chains can either point out towards the extracellular vestibule or point in towards the selectivity filter pore. Inward facing conformations, referred to as 'dunked' in this study, are shown to be favored in the presence of Na^+, and consequently promote Na^+ binding in the selectivity filter. The amalgamation of Na^+ ions and multiple carboxyl conformers, leads to an extensive plethora of favorable states. Dynamic transitions between these ionic clusters occur on a <100 ps timescale and resembling that of a highly disorded liquid. The lack of preference for a particular state, and the separation by low-lying barriers, therefore promotes diffusion in the selectivity filter and high throughput Na^+ permeation. The authors suggest voltage-driven non-equilibrium MD simulations may bias the dynamic behavior of the EEEE motif and discourage the occupation of degenerate conformational states in earlier studies, thereby overlooking this phenomenon.

Subsequently, Boiteux and coworkers identified a double potential well at S_{HFS} in PMF profiles, corresponding to available conformers of Glu177, reducing the barrier

between selectivity filter sites (Boiteux, Vorobyov, & Allen, 2014). An average occupancy of 2.3 ions is reported in the selectivity filter, lending further evidence to a three-ion conduction mechanism in which the selectivity filter switches between one, two and three-ion configurations facilitated by the isomerization of Glu177. In this case, three ion-binding events are promoted after the cleavage of H-bonding between Glu177 carbonyls and Ser178 hydroxyl groups, which restrict Glu177 movement during the first microsecond of the simulation. This remark illustrates that short scale MD simulations are also unlikely to sample this phenomena.

The coexistence of conduction mechanisms with 2 or 3 ions inside the selectivity filter was observed also in bias-exchange metadynamics simulations (Domene, Barbini & Furini, 2015). The significance of triply occupied states requires further investigation with regards to the possibility of contrasting mechanisms of Na^+ of inward and outward conduction. Comparative studies of Na_VAb (Stock, Delemotte, et al., 2013) and Na_VMs (Ke et al., 2014) channels under depolarized and hyperpolarized membrane potentials, to emulate influx and efflux respectively, have therefore been undertaken to elucidate this proposal.

Both studies displayed an increased maximum barrier to conduction (4.6 kcal/mol vs. 0.4 kcal/mol and 2.1 kcal/mol vs. 2.3 kcal/mol respectively) between S_{CEN} and S_{HFS}, with considerably higher dwell times in the selectivity filter (13.5±0.6 ns vs. 20.1±1.1 ns) and hence lower flux rates (15±3 pS vs. ~27±3 pS) in Na_VMs. Furthermore, an increased average occupancy of ~2.3 during efflux in comparison to ~1.8 ions during influx was observed in Na_VAb, thereby suggesting independent conduction mechanisms, with the presence of a third ion more predominant in the outward direction (Stock, Delemotte, et al., 2013).

An additional 'nudging' ion is observed to initiate the process in both systems. Therefore, to overcome the heightened barrier, this is considered to be an essential requirement. Moreover, in a Na_VMs study reversible rotations of Glu177 residues play a pivotal role in efflux (Ke et al., 2014). A significantly larger proportion of flipped states is observed resulting in appreciable differences in the distribution of the ions throughout the selectivity filter (32±5.9% vs. 2.7±0.5% for influx). Binding at

S_{HFS} was found to be generally on-axis in contrast to typical asymmetric binding. Furthermore, S_{CEN} and an intermediate region below S_{HFS} were more densely populated. Additional simulations with a restrained 'one-flip' ring conformation displayed increased efflux rates (relative to 'no-flip' simulations), reiterating these proposals, yet appeared uncoupled to the Na^+ influx rate, disagreeing with Chakrabarti's earlier conclusions that this phenomenon was essential for the catalysis of Na^+ permeation regardless of the directionality (Chakrabarti et al., 2013). The discrepancies between previous studies are attributed to use of an open-state structure, as opposed to closed Na_VAb, which will induce repulsive effects when the central cavity is inhabited, in conjunction with the use of different forcefields (Cordomí, Caltabiano, & Pardo, 2012).

4.3 Protonation State of Glu177

The conformational states of the EEEE signature sequence are further complicated by the prospect that one or more glutamate residues may be protonated. With potential implications for the electrostatics at the extracellular vestibule, and hence the ability to attract cations, and the overall structural stability of the selectivity filter and its enclosed binding sites, the dependency of the conduction mechanism on the protonation state requires thorough investigation.

Corry and Thomas (2012) calculated the 1D PMF profiles for Na_VAb with one and two Glu177 (in opposite side chains) residues protonated; the former exhibited a shallower, yet similar, profile with lower occupation of S_{HFS}, expected from the reduced negative potential of the selectivity filter. In contrast, when two protonated Glu177 residues are present, the ability of S_{HFS} to beckon Na^+ ions out of extracellular solution is diminished, in addition to an unexpectedly high energy at S_{CEN}, stunting Na^+ permeation.

Similar conclusions were reached from long scale MD simulations (Boiteux et al., 2014), suggesting an essentially barrierless (~1.5 kcal/mol maximum barrier to conduction) multi ion 'knock-on' or 'pass-by' mechanism is more likely in the fully charged state, promoted by repulsive interactions between charged side-chains. The presence of one protonated glutamate, similarly, leads to a reduced charged density

at the mouth of the selectivity filter. Rotational movements of Glu177 are integral in smoothing the energetic landscape and deeming conduction energetically feasible in this state, yet discourage three ion events in the selectivity filter suggesting permeation occurs to a less extent. When two or more residues are protonated, hydrogen bonds between protonated and deprotonated glutamates occlude the permeation pathway causing significant barriers in the plane of the EEEE motif. Intra-pore proton block, such as this has been identified experimentally in $Na_V1.4$ (Khan, Kyle, Hanck, Lipkind, & Fozzard, 2006) and selected L-type Ca^{2+} channels (Chen, Bezprozvanny, & Tsien, 1996).

Overall, it is apparent that systems containing multiple protonated glutamates are unfeasible states for ion conduction; a fully charged EEEE ring is optimal for conduction; yet, the structural and functional state of Na_VAb containing a single uncharged Glu177 is presently dubious. An additional study by Furini et al identified a noticeable increase in flexibility of the protonated glutamate relative to its deprotonated counterparts, residing in novel side chain conformations pointing towards S_{CEN} and laying at the back of the selectivity filter (Furini, Barbini & Domene, 2014). As a consequence, structural fluctuations throughout the entire selectivity filter were experienced, with a substantial impact in both 1D and 2D PMF's, the energetics of which are likely to markedly impede ion flow. Recognized differences with prior microsecond simulations are attributed to allowed transitions to alternative metastable states that are unlikely to be sampled during typically short umbrella sampling trajectories, employed in this study. The appropriateness of these methods to the question in hand remains ambiguous; therefore, the physiological relevance of identified structural and permeation properties of a singly protonated Na_V selectivity filter cannot be delineated at present.

An interesting observation worth noting, however, is the extent to which structural changes at the selectivity filter are propagated throughout the entire pore domain. Restriction of the selectivity filter, in a singly protonated system, seemingly adjusts the cavity shape and the orientation of S6 (Boiteux et al., 2014). The observed bent conformation in S6, on the level of P200–T206, is parallel to that of an inactivated

structure suggested by Payandah et al (Payandeh et al 2012). Such rapid conformational flux appears to be an inherent property of Na_V behavior on a microsecond timescale, potentially related to slow-inactivation (millisecond to second).

Structural rearrangements in this region also have implications for fenestrations between the central core and the surrounding membrane. The size of these openings is directly related to the activation state of S6; specifically, the rotation of F203 of phenyl side-chains reversibly blocks the pathway, consistent with experimental reports this residue is essential for inactivation and drug binding (Ahern, Eastwood, Dougherty, & Horn, 2008; Carboni, Zhang, Neplioueva, Starmer, & Grant, 2005; Li, Galue, Meadows, & Ragsdale, 1999; Ragsdale, McPhee, Scheuer, & Catterall, 1994). The open fenestrations have a maximum ~4 Å width, feasible for the entry of lipophilic drugs (i.e. local anesthetics), suggesting binding at this site may influence slow channel inactivation propagated through this region from the selectivity filter (Carboni et al., 2005; Z. Chen et al., 2000; Li et al., 1999).

4.4 Selectivity of Na^+ over other monovalent and divalent ions

To elucidate the molecular determinants of selectivity in Na^+ channels comparison of the energy profiles of Na^+ and K^+ was undertaken (Corry & Thomas, 2012; Furini & Domene, 2012). A similar landscape was observed, with elevated barriers at S_{HFS} and S_{CEN} of the order of 5-6 kcal/mol, independent of the presence of multiple ions.

Further analysis of the PMF displayed a similar binding affinity of both ions at S_{HFS}, due to flexibility and availability of water molecules, with a notable barrier to conduction arising in the plane of the Glu177 side chains. Corry et al. proposed a mechanism for this concerning the orientation of the proximal residues: The ideal geometry of S_{HFS}, during a binding event involves a straight ion-water-carbonyl complex. However, the increased distance of direct coordination between K^+ and Glu177 means this conformation is improbable unless reorganization of the binding site occurs. Only slight differences in the binding site size are observed, between K^+ and Na^+, insufficient for this purpose. Therefore, even though K^+ can fit through the pore with a full shell it is not in an optimum geometry.

This hypothesis was tested further by analysis of the relationship between selectivity and pore radius. The free energies of K^+, relative to Na^+, to travel through Glu177 ring of a model pore illustrated a lack of selectivity until bridging water molecules can no longer fit in plane of the pore, and a peak of selectivity at 6.3 Å, optimum for Na^+ and in plane binding of water molecules. Similar free energies are observed over a wide range of values, suggesting favorable conduction does not require specific alignment with the pore axis, as in K^+ channels.

In both studies (Corry & Thomas, 2012; Furini & Domene, 2012), the calculated energetic penalty of K^+ conduction through a Na_V channel was 3 kcal/mol, as opposed to 6 kcal/mol in the reverse situation of Na^+ conduction in K^+ channels. Therefore, the feasibility of K^+ conduction via this mechanism is consistent with the lower selectivity identified in Na_V channels compared to K^+ channels; K^+ channels select for K^+ ions at a rate of approximately 1000 to 1 whereas in Na^+ channels this is reduced to only 8 to 1.

The close relationship between Na^+ and Ca^{2+} selective channels complicates the situation of determining the origins of channel selectivity. A similar 4P/6TM architecture and selectivity filter structure, in addition to interchangeable selectivity in both channel families on the mutation of selected selectivity filter residues, suggests only subtle differences in protein structure are responsible for the observed conduction ratios (Heinemann, Terlau, Stuhmer, Imoto, & Numa, 1992b; Shaya et al., 2011; Sun et al., 1997a; Yue, Navarro, Ren, Ramos, & Clapham, 2002). The similar ionic radii leads to proposals that selectivity is based on the inability of Na^+-channels to accommodate the increased charge density of Ca^{2+} (Corry, 2013).

Similarly to comparative simulations of Na^+ and K^+ described above, off-axis binding modes between Glu177 and Ser178 are observed in the external site with Ca^{2+}, with an energetic barrier whilst penetrating the 'EEEE ring' (Corry, 2013). A ~3 kcal/mol energetic penalty (1 kcal/mol for Na^+) is observed accompanying movement from the selectivity filter to central cavity, emphasizing an increased binding affinity for Ca^{2+} in this site. Furthermore, an additional barrier was identified deeper into the pore before reaching the central/internal sites, in contrast to Na^+ and K^+. An average

lower coordination number observed at this position and corresponding energies of dehydration of about 8 kcal/mol, to reduce the coordination shell from seven to six, suggests the removal of water molecules is a feasible explanation of the energy barrier. The lack of ion-protein interactions, from the selectivity filter lining residues, to compensate for the reduced ion-water interactions further substantiates this claim. Increased affinity for water binding in Ca^{2+} is also observed in the second solvation shell, likely propagating this effect further. The presence of a second ion lowers the maximum barrier to conduction between S_{HFS} and S_{CEN} to ~4.5 kcal/mol; therefore an analogous weakly coupled 'knock on' mechanism is expected here. In a mixed ionic solution, barriers to Ca^{2+} conduction are slightly lower than those observed in the single-ion conduction. Na^{+} permeation, in the presence of bound Ca^{2+}, appears to be the most likely scenario in this case however, despite an increased barrier in comparison to Na^{+} alone, suggesting the presence of Ca^{2+} diminishes Na^{+} conduction. This is consistent with experimental reports of Ca^{2+} obstruction (French, Worley, Wonderlin, Kularatna, & Krueger, 1994; Ravindran, Schild, & Moczydlowski, 1991; Yamamoto, Yeh, & Narahashi, 1984) albeit to a considerably lesser extent than predicted computationally (Ren et al., 2001). The disparity is likely due to the uniform protonation states of Glu177 residues and limitations regarding the use of non-polarizable force fields for divalent cations (Bakó, Hutter, & Pálinkás, 2002; Bucher & Kuyucak, 2008).

Simulations undertaken simultaneously by Ke et al proposed contrasting conclusions (Ke, Zangerl, & Stary-Weinzinger, 2013). After a ~40 ns occupation of S_{HFS}, the ion entered an intermediate site below the EEEE ring, termed ($S_{S178/L176}$) in this study, formed from the backbone nitrogen's of S178 and L176, for a further 55 ns. The single ion entered S_{CEN} thereafter, which is populated for the remainder of the simulation, excluding the entrance of further ions. The general landscape of the PMF energy profile is in general agreement with those calculated by the Corry group for single-ion conduction. An elevated barrier is observed in the plane of the EEEE ring, suggesting discrimination against Ca^{2+} may occur in this region due to size constraints in a similar mechanism proposed for K^{+} selectivity (Corry & Thomas, 2012). In addition, a significant barrier is observed after S_{CEN}, suggesting diffusion into the

central cavity may be the rate-limiting step in the case of inward conduction of Ca^{2+}. The high binding affinity for S_{CEN} is consistent with crystallographic data of the closely related Na_VRh channel.

The presence of a potential well at $S_{S178/L176}$ requires further investigation; in this site, two rotated Glu177 residues bind Ca^{2+}, to optimize the available electrostatic network. When the ion vacates this site, one glutamate moved back to its original orientation, with the second revolving further to accommodate ion translocation to S_{CEN} demonstrating the flexibility of this residue in this case. Similar potential wells are observed in PMF profiles of Na^+ (Ke et al, 2013), Na^+ and K^+ (Furini & Domene, 2012) and Ca^{2+} (Boiteux et al., 2014) yet absent in analogous calculations of Na^+, K^+ and Ca^{2+} permeation (Corry & Thomas, 2012) highlighting further contentions in the literature concerning the behavior of Glu177.

In Na_VRh, all simulations with variable concentrations of Ca^{2+} show persistent binding at S1; strong binding determined by electrostatic interactions with Glu183, as well as interactions with S180 result in an insurmountable energy barrier (~11.38 kcal/mol), hindering progression deeper in the selectivity filter (Zhang et al., 2013). Therefore, the authors suggest this site confers selectivity in Na_VRh. The binding mode of Na^+ at S1 is reflective of preferred interactions with S181; this conformation is unreachable when Ca^{2+} is bound, consistent with extracellular millimolar blockage of Na^+ current by Ca^{2+}. Simulations with ions beginning in the central cavity were used to examine binding in S2. Here, Ca^{2+} exists preferentially in the center, approximately equidistant from the eight surrounding carbonyls. In contrast, Na^+ binds off-axis, in close proximity to one or two of the carbonyls, occasionally jumping between positions, subsequently persuading asymmetric selectivity filter conformations. Elements of asymmetry are observed to some extent throughout the entire Na^+ translocation process, despite the homologous sequence present in all subunits. Relative to other NaChBac channels, the selectivity filter sequence and asymmetric binding features of Na_VRh could be more applicable to mammalian Na_V channels, which contain non-conserved selectivity filter sequences; therefore, it is likely more studies utilizing this structure will emerge in the coming years.

5 Conclusions

In this review, we have primarily focused on the mechanisms of conduction and selectivity in Na^+-channels and a comparison with K^+-channels has been established. Aspects of voltage-gating and drug blockage have likewise been studied by computational methods to which numerous reviews are available (Bagnéris, Naylor, McCusker, & Wallace, 2015; Stock, Souza, & Treptow, 2013; Vargas et al., 2012). There is a general consensus about the main characteristics of ion conduction in bacterial Na^+-channels emerging from atomistic stimulations. Conduction requires the cooperative movement of at least two Na^+ ions across the selectivity filter of the channel. In sharp contrast to K^+-channels, the movements of the ions inside the selectivity filter of Na^+-channels are only loosely correlated, and the passage of water molecules is uncoupled from ion conduction. The central region of the selectivity filter can host a hydrated Na^+ ion but it cannot host a hydrated K^+ ion, which might explain the low selectivity of bacterial Na^+ channels for Na^+ ions over K^+ ions. In spite of this overall picture, there are still some controversial issues about the conformation of Glu177 and the number of ions involved in conduction events. Extensive atomistic simulations proved that the side chain of Glu177 is highly mobile, conferring a liquid-like nature to the selectivity filter of bacterial Na^+-channels. Instead, in other simulations of ion conduction, the side chain of Glu177 did not show significant deviations from the crystallographic structure. Therefore, the importance of the conformational states of Glu177 on ion conduction is still disputed. The movements of Glu177 can also modify the number of Na^+ ions inside the selectivity filter, and consequently the number of ions involved in conduction events. Conduction mechanisms with two and three ions have been observed, and it has been proposed that inward and outward conduction might follow different routes, having the third ion a more critical role in outward conduction. It is possible that several conduction mechanisms coexist for bacterial Na^+ channels, as it has been suggested for K^+-channels (Furini & Domene, 2009), and that the distribution of the conductive trajectories among these different mechanisms is influenced by the membrane potential and by the concentration of ions in the intracellular and extracellular compartments. These open questions can be investigated by atomistic

simulations, and they will provide a description of ion conduction in bacterial Na^+-channels at an unprecedented level of detail.

Acknowledgements. Work in the Domene lab is supported by the Hartree Center and the Engineering and Physical Sciences Research Council via the UK National Service for Computational Chemistry Software (NSCCS) and Archer. V.O. is supported by a CASE studentship from the Biotechnology and Biological Sciences Research Council and Pfizer Neusentis.

References

Ahern, C. A., Eastwood, A. L., Dougherty, D. A., & Horn, R. (2008). Electrostatic contributions of aromatic residues in the local anesthetic receptor of voltage-gated sodium channels. *Circ Res, 102*(1), 86-94.

Alcayaga, C., Cecchi, X., Alvarez, O., & Latorre, R. (1989). Streaming potential measurements in Ca^{2+}-activated K^+ channels from skeletal and smooth muscle. Coupling of ion and water fluxes. *Biophys J, 55*(2), 367-371.

Amaral, C., Carnevale, V., Klein, M. L., & Treptow, W. (2012). Exploring conformational states of the bacterial voltage-gated sodium channel NavAb via molecular dynamics simulations. *Proc Natl Acad Sci U S A, 109*(52), 21336-21341.

Ando, H., Kuno, M., Shimizu, H., Muramatsu, I., & Oiki, S. (2005). Coupled K^+-water flux through the HERG potassium channel measured by an osmotic pulse method. *J Gen Physiol, 126*(5), 529-538.

Aqvist, J., Luecke, H., Quiocho, F. A., & Warshel, A. (1991). Dipoles localized at helix termini of proteins stabilize charges. *Proc Natl Acad Sci U S A, 88*(5), 2026-2030.

Aqvist, J., & Luzhkov, V. (2000). Ion permeation mechanism of the potassium channel. *Nature, 404*(6780), 881-884.

Bagal, S. K., Brown, A. D., Cox, P. J., Omoto, K., Owen, R. M., Pryde, D. C., Swain, N. A. (2013). Ion Channels as Therapeutic Targets: A Drug Discovery Perspective. *J Med Chem, 56*(3), 593-624.

Bagnéris, C., DeCaen, P. G., Hall, B. A., Naylor, C. E., Clapham, D. E., Kay, C. W. M., & Wallace, B. A. (2013). Role of the C-terminal domain in the structure and function of tetrameric sodium channels. *Nat Commun, 4*.

Bagnéris, C., Naylor, C. E., McCusker, E. C., & Wallace, B. A. (2015). Structural model of the open–closed–inactivated cycle of prokaryotic voltage-gated sodium channels. *J Gen Physiol, 145*(1), 5-16.

Bakó, I., Hutter, J., & Pálinkás, G. (2002). Car–Parrinello molecular dynamics simulation of the hydrated calcium ion. *J Chem Phys, 117*(21), 9838-9843.

Begenisich, T. B., & Cahalan, M. D. (1980). Sodium channel permeation in squid

axons. I: Reversal potential experiments. *J Physiol, 307*, 217-242.

Benos, D. J., Hyde, B. A., & Latorre, R. (1983). Sodium flux ratio through the amiloride-sensitive entry pathway in frog skin. *J Gen Physiol, 81*(5), 667-685.

Berendsen, H. J. C., van der Spoel, D., & van Drunen, R. (1995). GROMACS: A message-passing parallel molecular dynamics implementation. *Comp Phys Comm, 91*(1–3), 43-56.

Berneche, S., & Roux, B. (2001). Energetics of ion conduction through the K^+ channel. *Nature, 414*(6859), 73-77.

Bernèche, S., & Roux, B. (2000). Molecular dynamics of the KcsA K^+ channel in a bilayer membrane. *Biophys J, 78*(6), 2900-2917.

Bezanilla, F., & Armstrong, C. M. (1972). Negative conductance caused by entry of sodium and cesium ions into the potassium channels of squid axons. *J Gen Physiol, 60*(5), 588-608.

Black, J. A., & Waxman, S. G. (2013). Noncanonical roles of voltage-gated sodium channels. *Neuron, 80*(2), 280-291.

Boiteux, C., Vorobyov, I., & Allen, T. W. (2014). Ion conduction and conformational flexibility of a bacterial voltage-gated sodium channel. *Proc Natl Acad Sci U S A, 111*(9), 3454-3459.

Brohawn, del Marmol, J., & MacKinnon, R. (2012). Crystal structure of the human K2P TRAAK, a lipid- and mechano-sensitive K^+ ion channel. *Science, 335*, 436-441.

Brooks, B. R., Bruccoleri, R. E., Olafson, B. D., States, D. J., Swaminathan, S., & Karplus, M. (1983). CHARMM: A program for macromolecular energy, minimization, and dynamics calculations. *J Comput Chem, 4*(2), 187-217.

Bucher, D., & Kuyucak, S. (2008). Polarization of water in the first hydration shell of K^+ and Ca^{2+} ions. *J Phys Chem B, 112*(35), 10786-10790.

Carboni, M., Zhang, Z. S., Nepliouéva, V., Starmer, C. F., & Grant, A. O. (2005). Slow sodium channel inactivation and use-dependent block modulated by the same domain IV S6 residue. *J Membr Biol, 207*(2), 107-117.

Carnevale, V., Treptow, W., & Klein, M. L. (2011). Sodium Ion Binding Sites and Hydration in the Lumen of a Bacterial Ion Channel from Molecular Dynamics Simulations. *J Phys Chem Lett, 2*(19), 2504-2508.

Chakrabarti, N., Ing, C., Payandeh, J., Zheng, N., Catterall, W. A., & Pomès, R. (2013). Catalysis of Na^+ permeation in the bacterial sodium channel NaVAb. *Proc Natl Acad Sci U S A, 110*(28), 11331-11336.

Chen, Bezprozvanny, I., & Tsien, R. W. (1996). Molecular basis of proton block of L-type Ca^{2+} channels. *J Gen Physiol, 108*(5), 363-374.

Chen, Z., Ong, B.-H., Kambouris, N. G., Marbán, E., Tomaselli, G. F., & Balser, J. R. (2000). Lidocaine induces a slow inactivated state in rat skeletal muscle sodium channels. *J Physiol, 524*, 37-49.

Cordero-Morales, J. F., Jogini, V., Chakrapani, S., & Perozo, E. (2011). A Multipoint Hydrogen-Bond Network Underlying KcsA C-Type Inactivation. *Biophys J, 100*(10), 2387-2393.

Cordomí, A., Caltabiano, G., & Pardo, L. (2012). Membrane Protein Simulations Using AMBER Force Field and Berger Lipid Parameters. *J Chem Theory Comput, 8*(3), 948-958.

Cornell, W. D., Cieplak, P., Bayly, C. I., Gould, I. R., Merz, K. M., Ferguson, D. M., . . . Kollman, P. A. (1995). A Second Generation Force Field for the Simulation of Proteins, Nucleic Acids, and Organic Molecules. *J Am Chem Soc, 117*(19), 5179-5197.

Corry, B. (2013). Na^+/Ca^{2+} selectivity in the bacterial voltage-gated sodium channel NavAb. *PeerJ, 1*, e16.

Corry, B., & Thomas, M. (2012). Mechanism of Ion Permeation and Selectivity in a Voltage Gated Sodium Channel. *J Am Chem Soc, 134*(3), 1840-1846.

Cuello, L. G., Jogini, V., Cortes, D. M., & Perozo, E. (2010). Structural mechanism of C-type inactivation in K^+ channels. *Nature, 466*(7303), 203-208.

Domene, C., Klein, M. L., Branduardi, D., Gervasio, F. L., & Parrinello, M. (2008). Conformational changes and gating at the selectivity filter of potassium channels. *J Am Chem Soc, 130*(29), 9474-9480.

Domene, C., & Sansom, M. S. (2003). Potassium channel, ions, and water: simulation studies based on the high resolution X-ray structure of KcsA. *Biophys J, 85*(5), 2787-2800.

Doyle, D. A., Morais Cabral, J., Pfuetzner, R. A., Kuo, A., Gulbis, J. M., Cohen, S. L., . . . MacKinnon, R. (1998). The structure of the potassium channel: molecular basis of K^+ conduction and selectivity. *Science, 280*(5360), 69-77.

Eisenman, G. (1962). Cation Selective Glass Electrodes and their Mode of Operation. *Biophys J, 2*, 259-323.

Eisenman, G., & Horn, R. (1983). Ionic selectivity revisited: The role of kinetic and equilibrium processes in ion permeation through channels. *J Membr Biol, 76*(3), 197-225.

England, S., & de Groot, M. J. (2009). Subtype-selective targeting of voltage-gated sodium channels. *Br J Pharmacol, 158*(6), 1413-1425.

Favre, I., Moczydlowski, E., & Schild, L. (1996). On the structural basis for ionic selectivity among Na^+, K^+, and Ca^{2+} in the voltage-gated sodium channel. *Biophys J, 71*, 3110-3125.

French, R. J., Worley, J. F., Wonderlin, W. F., Kularatna, A. S., & Krueger, B. K. (1994). Ion permeation, divalent ion block, and chemical modification of single sodium channels. Description by single- and double-occupancy rate-theory models. *J Gen Physiol, 103*, 447-470.

Furini, S., Beckstein, O., & Domene, C. (2009). Permeation of water through the KcsA K^+ channel. *Proteins, 74*(2), 437-448.

Furini, S. & Domene, C. (2009). Atypical mechanism of conduction in potassium

channels. *Proc Natl Acad Sci U S A, 106*(38), 16074-16077.

Furini, & Domene, C. (2012). On conduction in a bacterial sodium channel. *PLoS Comput Biol, 8*(4), e1002476.

Furini, S., & Domene, C. (2013). K^+ and Na^+ Conduction in Selective and Nonselective Ion Channels Via Molecular Dynamics Simulations. *Biophys J, 105*(8), 1737-1745.

Furini, S., Zerbetto, F., & Cavalcanti, S. (2007). Role of the intracellular cavity in potassium channel conductivity. *J Phys Chem B, 111*(50), 13993-14000.

Gilchrist, J., Das, S., Van Petegem, F., & Bosmans, F. (2013). Crystallographic insights into sodium-channel modulation by the β4 subunit. *Proc Natl Acad Sci U S A, 110*(51), E5016-E5024.

Heginbotham, L., Lu, Z., Abramson, T., & MacKinnon, R. (1994). Mutations in the K^+ channel signature sequence. *Biophys J, 66*(4), 1061-1067.

Heinemann, S. H., Terlau, H., Stuhmer, W., Imoto, K., & Numa, S. (1992). Calcium channel characteristics conferred on the sodium channel by single mutations. *Nature, 356*, 441-443.

Hille, B. (1971). The permeability of the sodium channel to organic cations in myelinated nerve. *J Gen Physiol, 58*(6), 599-619.

Hille, B. (1972). The permeability of the sodium channel to metal cations in myelinated nerve. *J Gen Physiol, 59*(6), 637-658.

Hille, B. (1992). *Ionic Channels of Excitable Membranes* (2nd ed.). Sunderland, Mass.: Sinauer Associates Inc.

Hodgkin, A. L., & Keynes, R. D. (1955). The potassium permeability of a giant nerve fibre. *J Physiol, 128*(1), 61-88.

Illingworth, C. J., & Domene, C. (2009). Many-body effects and simulations of potassium channels. *Proc Roy Soc A, 465*(2106), 1701-1716.

Jensen, M. Ø., Jogini, V., Borhani, D. W., Leffler, A. E., Dror, R. O., & Shaw, D. E. (2012). Mechanism of Voltage Gating in Potassium Channels. *Science, 336*(6078), 229-233.

Jiang, Y., Lee, A., Chen, J., Ruta, V., Cadene, M., Chait, B. T., & MacKinnon, R. (2003). X-ray structure of a voltage-dependent K^+ channel. *Nature, 423*(6935), 33-41.

Jogini, V., & Roux, B. (2005). Electrostatics of the intracellular vestibule of K^+ channels. *J Mol Biol, 354*(2), 272-288.

Jorgensen, W. L., & Tirado-Rives, J. (1988). The OPLS [optimized potentials for liquid simulations] potential functions for proteins, energy minimizations for crystals of cyclic peptides and crambin. *J Am Chem Soc, 110*(6), 1657-1666.

Ke, Timin, E. N., & Stary-Weinzinger, A. (2014). Different inward and outward conduction mechanisms in NaVMs suggested by molecular dynamics simulations. *PLoS Comput Biol, 10*(7), e1003746.

Ke, Zangerl, E.-M., & Stary-Weinzinger, A. (2013). Distinct interactions of Na^+ and Ca^{2+} ions with the selectivity filter of the bacterial sodium channel NaVAb. *Biochem Biophys Res Commun, 430*(4), 1272-1276.

Khan, A., Kyle, J. W., Hanck, D. A., Lipkind, G. M., & Fozzard, H. A. (2006). Isoform-dependent interaction of voltage-gated sodium channels with protons. *J Physiol, 576*, 493-501.

Kuo, A., Gulbis, J. M., Antcliff, J. F., Rahman, T., Lowe, E. D., Zimmer, J., Doyle, D. A. (2003). Crystal structure of the potassium channel KirBac1.1 in the closed state. *Science, 300*(5627), 1922-1926.

Li, H. L., Galue, A., Meadows, L., & Ragsdale, D. S. (1999). A molecular basis for the different local anesthetic affinities of resting versus open and inactivated states of the sodium channel. *Mol Pharmacol, 55*(1), 134-141.

Long, S. B., Campbell, E. B., & Mackinnon, R. (2005). Crystal structure of a mammalian voltage-dependent Shaker family K^+ channel. *Science, 309*(5736), 897-903.

Long, S. B., Tao, X., Campbell, E. B., & MacKinnon, R. (2007). Atomic structure of a voltage-dependent K^+ channel in a lipid membrane-like environment. *Nature, 450*(7168), 376-382.

Luzhkov, V. B., & Åqvist, J. (2001). K^+/Na^+ selectivity of the KcsA potassium channel from microscopic free energy perturbation calculations. *BBA - Prot Struct Mol Enzymology, 1548*(2), 194-202.

Mantegazza, M., Curia, G., Biagini, G., Ragsdale, D. S., & Avoli, M. (2010). Voltage-gated sodium channels as therapeutic targets in epilepsy and other neurological disorders. *Lancet Neurol, 9*(4), 413-424.

McCusker, E. C., Bagneris, C., Naylor, C. E., Cole, A. R., D'Avanzo, N., Nichols, C. G., & Wallace, B. A. (2012). Structure of a bacterial voltage-gated sodium channel pore reveals mechanisms of opening and closing. *Nat Commun, 3*, 1102.

Miller, & Long. (2012). Crystal Structure of the Human Two–Pore Domain Potassium Channel K2P1. *Science, 335*(6067), 432-436.

Morais-Cabral, J. H., Zhou, Y., & MacKinnon, R. (2001). Energetic optimization of ion conduction rate by the K^+ selectivity filter. *Nature, 414*(6859), 37-42.

Namadurai, S., Balasuriya, D., Rajappa, R., Wiemhöfer, M., Stott, K., Klingauf, J.,. Jackson, A. P. (2014). Crystal Structure and Molecular Imaging of the Nav Channel β3 Subunit Indicates a Trimeric Assembly. *J Biol Chem, 289*(15), 10797-10811.

Noda, M., Shimizu, S., Tanabe, T., Takai, T., Kayano, T., Ikeda, T., et al. (1984). Primary structure of Electrophorus electricus sodium channel deduced from cDNA sequence. *Nature, 312*(5990), 121-127.

Noskov, S. Y., & Roux, B. (2006). Ion selectivity in potassium channels. *Biophys Chem, 124*(3), 279-291.

Parsegian, A. (1969). Energy of an Ion crossing a Low Dielectric Membrane:

Solutions to Four Relevant Electrostatic Problems. *Nature, 221*(5183), 844-846.

Payandeh, & Minor Jr, D. L. (2015). Bacterial Voltage-Gated Sodium Channels (BacNaVs) from the Soil, Sea, and Salt Lakes Enlighten Molecular Mechanisms of Electrical Signaling and Pharmacology in the Brain and Heart. *J Mol Biol, 427*(1), 3-30.

Payandeh, Scheuer, T., Zheng, N., & Catterall, W. A. (2011). The crystal structure of a voltage-gated sodium channel. *Nature, 475*(7356), 353-358.

Payandeh, J., Gamal El-Din, T. M., Scheuer, T., Zheng, N., & Catterall, W. A. (2012). Crystal structure of a voltage-gated sodium channel in two potentially inactivated states. *Nature, 486*(7401), 135-139.

Qiu, H., Shen, R., & Guo, W. (2012). Ion solvation and structural stability in a sodium channel investigated by molecular dynamics calculations. *Biochim Biophys Acta, 1818*(11), 2529-2535.

Ragsdale, D. S., McPhee, J. C., Scheuer, T., & Catterall, W. A. (1994). Molecular determinants of state-dependent block of Na^+ channels by local anesthetics. *Science, 265*(5179), 1724-1728.

Ravindran, A., Schild, L., & Moczydlowski, E. (1991). Divalent cation selectivity for external block of voltage-dependent Na^+ channels prolonged by batrachotoxin. Zn^{2+} induces discrete substates in cardiac Na+ channels. *J Gen Physiol, 97*(1), 89-115.

Ren, D., Navarro, B., Xu, H., Yue, L., Shi, Q., & Clapham, D. E. (2001). A Prokaryotic Voltage-Gated Sodium Channel. *Science, 294*(5550), 2372-2375.

Roux, B. (2005). Ion Conduction and Selectivity in K^+ Channels. *Ann Rev Biophys Biomol Struct, 34*(1), 153-171.

Shaya, D., Findeisen, F., Abderemane-Ali, F., Arrigoni, C., Wong, S., Nurva, S. R., . Minor Jr, D. L. (2014). Structure of a Prokaryotic Sodium Channel Pore Reveals Essential Gating Elements and an Outer Ion Binding Site Common to Eukaryotic Channels. *J Mol Biol, 426*(2), 467-483.

Shaya, D., Kreir, M., Robbins, R. A., Wong, S., Hammon, J., Brüggemann, A., & Minor, D. L. (2011). Voltage-gated sodium channel (NaV) protein dissection creates a set of functional pore-only proteins. *Proc Natl Acad Sci U S A, 108*(30), 12313-12318.

Smart, O. S., Goodfellow, J. M., & Wallace, B. A. (1993). The pore dimensions of gramicidin A. *Biophys Jl, 65*(6), 2455-2460.

Stock, L., Delemotte, L., Carnevale, V., Treptow, W., & Klein, M. L. (2013). Conduction in a Biological Sodium Selective Channel. *J Phys Chem B, 117*(14), 3782-3789.

Stock, L., Souza, C., & Treptow, W. (2013). Structural Basis for Activation of Voltage-Gated Cation Channels. *Biochemistry, 52*(9), 1501-1513.

Stuhmer, W., Conti, F., Suzuki, H., Wang, X., Noda, M., Yahagi, N., Numa, S. (1989). Structural parts involved in activation and inactivation of the sodium

channel. *Nature, 339*(6226), 597-603.

Sun, Y. M., Favre, I., Schild, L., & Moczydlowski, E. (1997a). On the structural basis for size-selective permeation of organic cations through the voltage-gated sodium channel. Effect of alanine mutations at the DEKA locus on selectivity, inhibition by Ca^{2+} and H^{+}, and molecular sieving. *J Gen Physiol, 110*, 693-715.

Sun, Y. M., Favre, I., Schild, L., & Moczydlowski, E. (1997b). On the structural basis for size-selective permeation of organic cations through the voltage-gated sodium channel. Effect of alanine mutations at the DEKA locus on selectivity, inhibition by Ca^{2+} and H^{+}, and molecular sieving. *J Gen Physiol, 110*(6), 693-715.

Ulmschneider, M. B., Bagnéris, C., McCusker, E. C., DeCaen, P. G., Delling, M., Clapham, D. E., . . . Wallace, B. A. (2013). Molecular dynamics of ion transport through the open conformation of a bacterial voltage-gated sodium channel. *Proc Natl Acad Sci U S A, 110*(16), 6364-6369.

Vanommeslaeghe, K., & MacKerell Jr, A. D. (2015). CHARMM additive and polarizable force fields for biophysics and computer-aided drug design. *BBA, 1850*(5), 861-871.

Vargas, E., Yarov-Yarovoy, V., Khalili-Araghi, F., Catterall, W. A., Klein, M. L., Tarek, M., Roux, B. (2012). An emerging consensus on voltage-dependent gating from computational modeling and molecular dynamics simulations. *J Gen Physiol, 140*(6), 587-594.

Vora, T., Corry, B., & Chung, S. H. (2008). Brownian dynamics study of flux ratios in sodium channels. *Eur Biophys J, 38*(1), 45-52.

Xu, P., Wang, J., Xu, Y., Chu, H., Liu, J., Zhao, M., . . . Li, G. (2015). Advancement of Polarizable Force Field and Its Use for Molecular Modeling and Design. In D. Wei, Q. Xu, T. Zhao, & H. Dai (Eds.), *Advance in Structural Bioinformatics* (Vol. 827, pp. 19-32): Springer Netherlands.

Yamamoto, D., Yeh, J. Z., & Narahashi, T. (1984). Voltage-dependent calcium block of normal and tetramethrin-modified single sodium channels. *Biophys J, 45*(1), 337-344.

Yue, L., Navarro, B., Ren, D., Ramos, A., & Clapham, D. E. (2002). The cation selectivity filter of the bacterial sodium channel, NaChBac. *J Gen Physiol, 120*, 845-853.

Zaydman, M. A., Silva, J. R., & Cui, J. (2012). Ion Channel Associated Diseases: Overview of Molecular Mechanisms. *Chem Rev, 112*(12), 6319-6333.

Zhang, X., Ren, W., DeCaen, P., Yan, C., Tao, X., Tang, L., Yan, N. (2012). Crystal structure of an orthologue of the NaChBac voltage-gated sodium channel. *Nature, 486*(7401), 130-134.

Zhang, X., Ren, W., DeCaen, P., Yan, C., Tao, X., Tang, L., Yan, N. (2012). Crystal structure of an orthologue of the NaChBac voltage-gated sodium channel. *Nature, 486*(7401), 130-134.

Zhang, X., Xia, M., Li, Y., Liu, H., Jiang, X., Ren, W., Gong, H. (2013). Analysis of the selectivity filter of the voltage-gated sodium channel NavRh. *Cell Res, 23*(3), 409-422.

Zhou, Morais-Cabral, Kaufman, & MacKinnon. (2001). Chemistry of ion coordination and hydration revealed by a K^+ channel-Fab complex at 2.0 angstrom resolution. *Nature, 414*, 43-48.

FIGURES

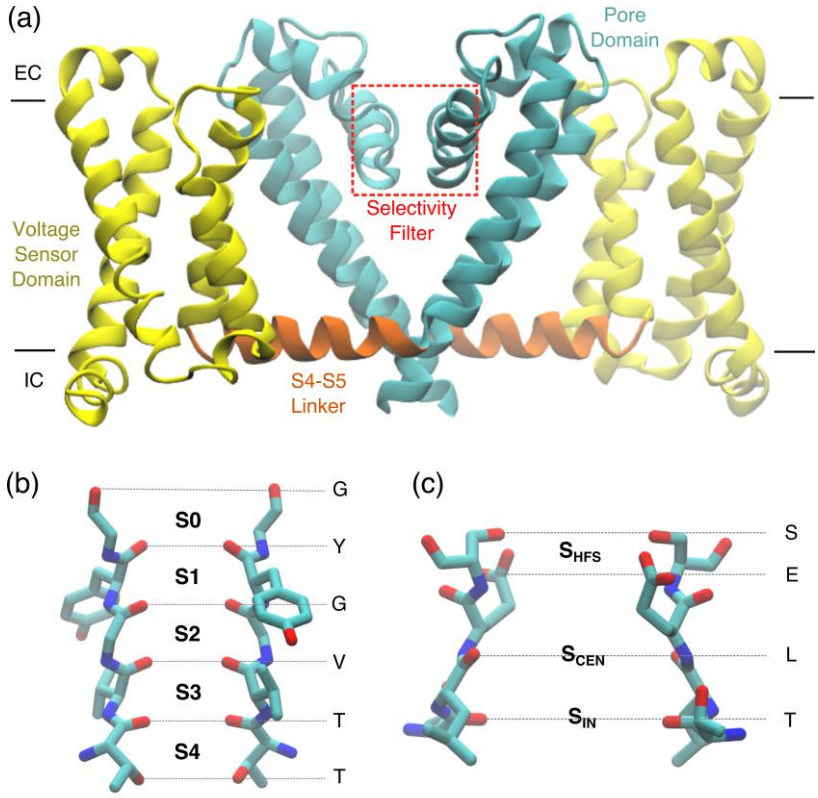

Figure 1. (a) Overall architecture of a voltage-gated ion channel as represented by the crystal structure of Na_VAb (PDB ID: 3RVY) in a closed conformation. Only two chains are shown for clarity. The VSD comprises transmembrane helices S1-S4, with S5 and S6 constituting the pore domain (PD) in cyan; the S4-S5 linker (in orange) is responsible for conferring conformational changes between the VSD and the PD on voltage activation. The selectivity filter is an integral part of the PD at the extracellular entrance to the pore. (b) Structure of a K^+ selective selectivity filter from the prototypical K^+ channel, KcsA (PDB ID: 1K4C). Binding sites are clearly defined by surrounding carbonyl oxygen atoms directed toward the pore axis. (c) Structure of a prototypical Na^+ selective selectivity filter from Na_VAb (PDB ID:3RVY), with proposed binding sites labeled.

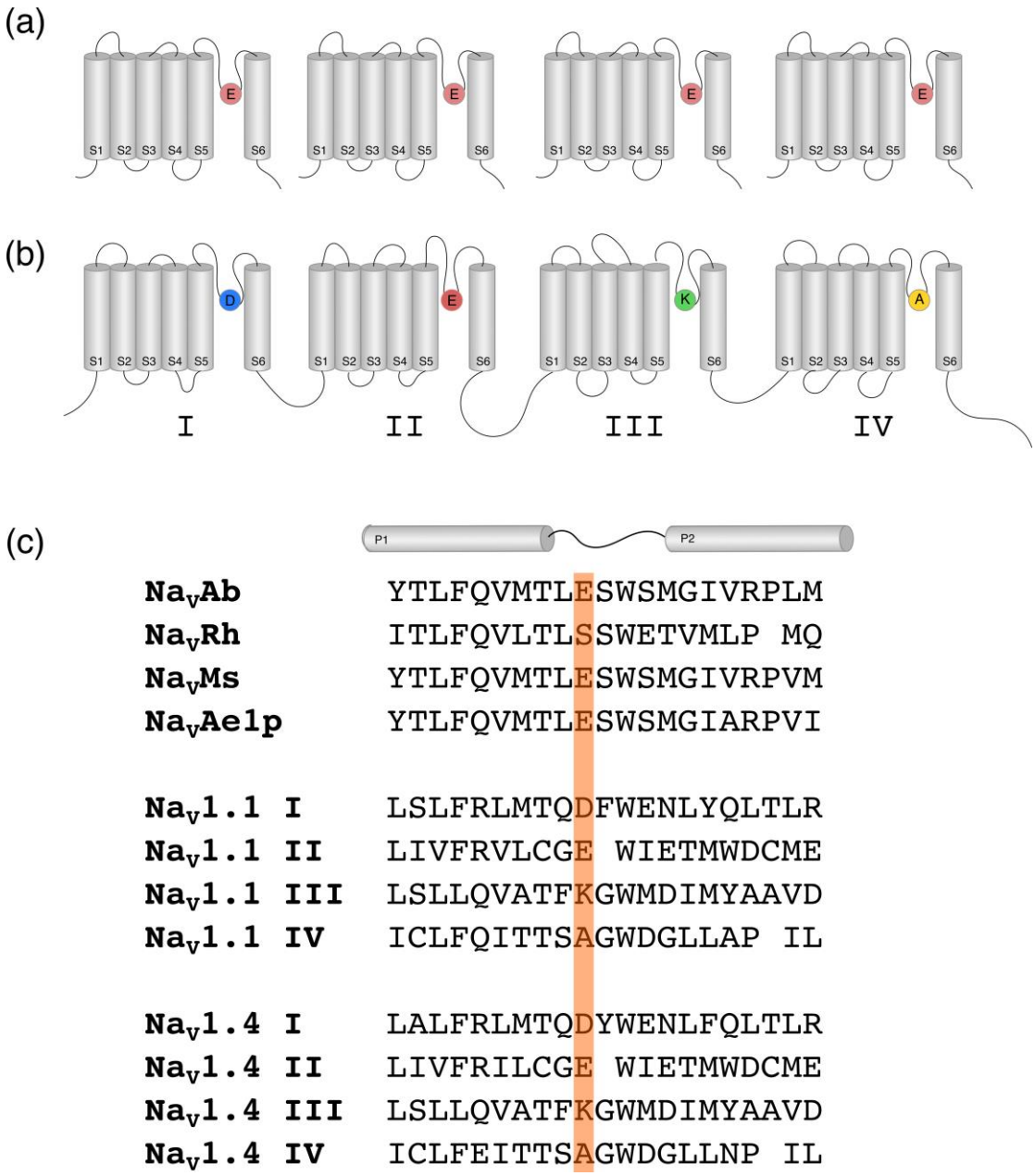

Figure 2. Topology and sequence data of voltage-gated sodium channels from prokaryotic and eukaryotic origins. (a) General representation of Na_V channel architecture from bacterial channels: four homologous subunits comprising voltage-sensor (S1-S4) and pore-forming (S5-S6) domains, containing the signature EEEE sequence, form the channel. (b) Eukaryotic channels share a similar tetrameric architecture, yet in a continuous a polypeptide chain, with non-conserved sequences in individual domains. In this case, DEKA constitutes the characteristic SF ring, as illustrated in (c). Sequence alignments of the selectivity filter and surrounding pore domain in select bacterial (Na_VAb, Na_VRh, Na_VMs, NaVAe1p) and mammalian (Na_V1.1, Na_V1.4) channels; the signature SF sequence is highlighted in orange (Payandeh & Minor Jr, 2015).

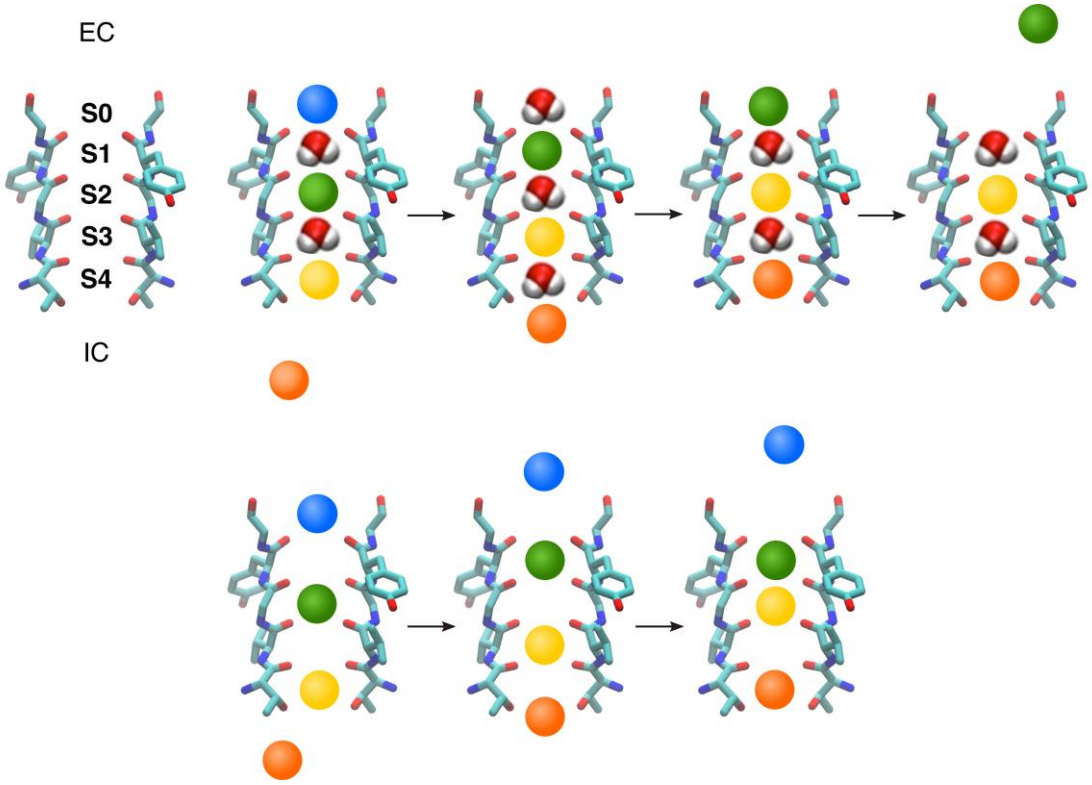

Figure 3. Proposed mechanisms of ion conduction in K^+ channels: (upper panel) chains of alternating K^+ ions and water molecules cross the selectivity filter, and/or (lower panel) cation move through the selectivity filter without intervening water molecules. Colored spheres represent individual K^+ ions. Approach of an ion from the central cavity prompts simultaneous ion movement throughout the selectivity filter, resulting in the exit of one ion that rapidly diffuses into the extracellular solution. The initial/final configuration of the selectivity filter was confirmed to be the most energetically favorable state using FEP methods (Aqvist & Luzhkov, 2000; Furini & Domene, 2009).

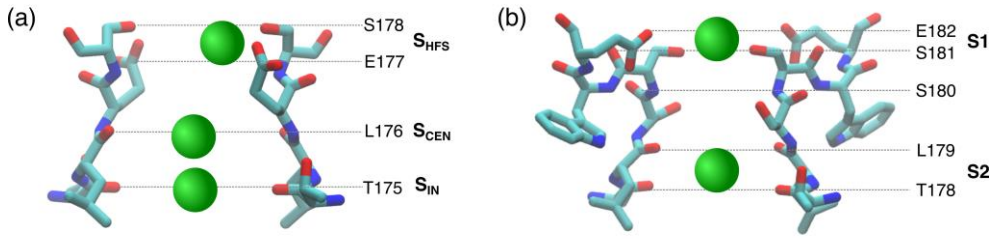

Figure 4. Binding sites in the selectivity filter of a Na^+-channel confirmed by MD simulations in (a) Na_VAb and (b) Na_VRh. Analogous binding sites as Na_VAb were also identified in Na_VMs.

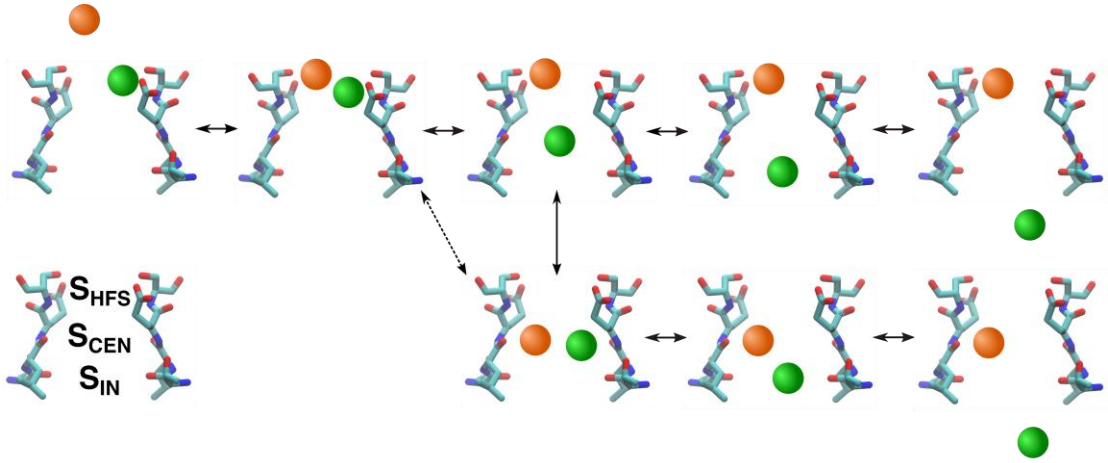

Figure 5. Proposed conduction pathways in the presence of two Na^+ ions in the selectivity filter. Selectivity filter residues are represented in licorice and Na^+ ions are orange and green spheres. 2D PMF profiles (Corry & Thomas, 2012; Furini & Domene, 2012) considering the position of individual ions along the pore axis, identified the minimum energy pathway following the sequence extracellular/S_{HFS}, S_{HFS}/S_{HFS}, S_{HFS}/S_{CEN}, S_{HFS}/S_{IN}, S_{HFS}/intracellular, represented in the upper array. Stock et al (Stock, Delemotte, et al., 2013) proposed an alternative mechanism with ions sequentially occupying extracellular/S_{HFS}, S_{HFS}/S_{HFS}, S_{HFS}/S_{CEN}, S_{CEN}/S_{CEN}, S_{CEN}/S_{IN} and S_{HFS}/intracellular. The latter proved predominant in accompanying voltage driven MD simulations.